Earthquake Geotechnical Engineering for Protection and Development of Environment and Constructions – Silvestri & Moraci (Eds)
© 2019 Associazione Geotecnica Italiana, Rome, Italy, ISBN 978-0-367-14328-2

The mechanism of liquefaction-triggered landslides under the coupling effect of the Minxian-Zhangxian Ms6.6 earthquake and rainfall in 2013

L.M. Wang, Q. Wang, K. Liu & J.C. Chen
Lanzhou Institute of Seismology, China Earthquake Administration, Lanzhou, China

Z.J. Wu
College of Transportation Science & Engineering, Nanjing Tech University, Nanjing, China

ABSTRACT: A strong earthquake with a magnitude of Ms6.6 occurred in the boundary between Minxian and Zhangxian counties in Gansu province, China on July 22, 2013. There were about 2330 landslides to be triggered by the earthquake. The largest and most serious landslide slid forward for about 1 km, buried a village and killed 12 people in Yongguang village. In this paper, based on field investigation, the topography and soil layer distribution of the west Yongguang loess landslide were identified. The mechanism of liquefaction-triggered landslide was investigated through dynamic triaxial torsional tests and shear wave velocity measurements. The results show that the landslides in Yongguang village was triggered by liquefaction under the coupling effect of the earthquake and rainfall.

1 INTRODUCTION

An earthquake measuring Ms6.6, focal depth of 20km, occurred at the junction of Minxian county and Zhangxian county, Dingxi City, Gansu Province, on July 22, 2013, which caused 95 people dead, 2414 people injured and an economic loss of more than US$5 billon. The epicenter is located in the transitional zone from the Gannan Plateau to the Loess Plateau and the Longnan Mountains, where is in the northeast margin of Qinghai-Tibet Plateau. The geological structure is complex, there are undulating mountains and crisscrossing rivers. The seismic geotechnical hazards including 2330 landslides and collapses as well as subsidence in tens sites developed in the meizoseismal zone (VIII degree) and its surrounding area (VII degree). The disasters show the characteristics of piece-wise and dense distribution, and have similar linear characteristics in macroscopic geographical distribution. Most of the secondary geotechnical disasters triggered by the earthquake are loess collapses, including some medium-deep landslides and mudflow. The field investigation shown that the distribution area of landslide concentrated area is mainly in the belt of connecting 7 villages, ChaGuTan, MaJiaGou, WenDou, CheLu, YongGuang, YongXing, and LaLu, with about 30 km long and about 8 km wide (Figure 1). The long axis of the strip in the densely distributed area of the landslide is consistent with the trend of the seismigenic structure (Wang et al. 2013; Wang et al. 2017).

These landslides buried villages, blocked roads and damaged power supply and communication cables. The most serious one is the mud-flow landslide triggered during the earthquake in the west of Yongguang Village. And the longest slip distance is about 1km, which buried 8 families of farmers, resulting in 12 deaths. The site conditions of the landslide body and the physical properties of the soil were analyzed, and the conditions of liquefaction of landslide soil and the possibility of liquefaction during earthquake were investigated using site survey, soil sampling, surface wave survey and dynamic triaxial liquefaction test. Combined with the dynamic finite element method and the strength reduction method, the influencing factors and the mechanism of the loess landslide were analyzed.

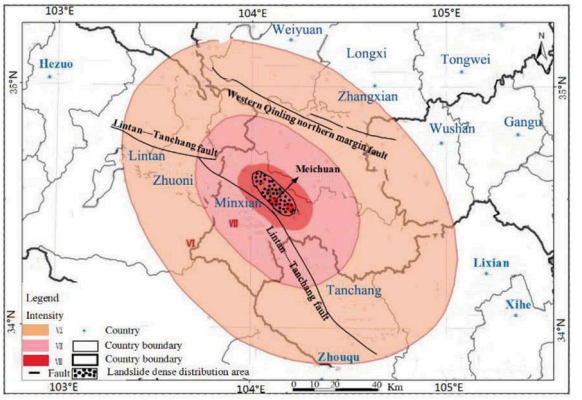

Figure 1. The earthquake intensity distribution and landslide densely distributed area.

2 CHARACTERISTICS OF LOESS LANDSLIDES AT YONGGAUNG VILLAGE

The landslide of western Yongguang Village looks like L-shape on the plane and runs nearly from north to south (Figure 2). It is found that the landslide is the internal slip in the soil layer of Malan loess formed in Q_3, with uneven silty content and thicker overburden. The water content of the soil is 24.53%, which is between the plastic limit and the liquid limit. The sliding body has a continuous distribution in the range from the back wall to the front edge of the landslide. It can be seen from the morphology of the soil that the landslide has strong fluidity during slippage. The back wall of the landslide is about 100 meters wide and 18 meters high. The thickness of sliding soil layer is about 15 meters on average. The width of the landslide body at the front edge is about 13 meters at the exit of the gully, and its maximum slip distance is about 1 km. The front edge of the mudflow is about 0.5 m away from the bridge foundation, where is at the gully exit (Figure 3). The overall drop of the landslide is about 253 m, and the average slope is 18°. The sliding soil body is about 400,000 m^3, which covered an area of 42,000 m^2.

The landslide broke through the original concave terrain and slid into a large gully with an angle of about 30 degrees. It slid downstream and ends in front of the arch bridge at the north side of bifurcation intersection of Yongguang and Yongxing. In the position where the landslide soil enters the gully, the mound formed by the sliding body was obviously visible. And part of the mudflow tracebacked to the upstream of the gully with the maximum distance of about 20 meters. The solifluction tracebacking is related to the mudflow and the drop at the bottom of the upstream of the gully. The size of the tracebacking mudflow was small, indicating that the mudflow was moving faster, which was coincident with the situation known to the local residents during the site visit.

Figure 2. Aerial image of Yongguang landslides.

Figure3. The front edge of the landslide.

3 HIGH-DENSITY SURFACE WAVE EXPLORATION OF LANDSLIDE SOIL

In order to obtain the underground Vs structure of the landslide, a survey line is set on the top of the mudflow landslide on the west side of Yongguang, as shown in Figure 2. The high-density surface wave line consists of 24 geophones with a sampling interval of 1ms and a recording time of 2.046s. Three excitations with offset of 10m, 15m and 20m are carried out respectively, and 12 moving intervals are arranged.

Sensors are equipped with 4.5 Hz moving coil vertical component velocity geophone. Geode digital high precision broadband seismograph (1.75 Hz ~ 20,000 Hz) is used for recording equipment. The vibration of surface wave exploration is generated by hammering method. The velocity scanning method is used to extract the dispersion curve from the multi-channel waveform records. The inverse analysis of dispersion curve is carried out using a hybrid algorithm (Yamanaka and Ishida 1996; Xi et al. 2018), which combines least square method and genetic algorithm. The approximate error of the dispersion curve is about 2% in the calculation.

The inversion results in Figure 4 and the profile of the landslide in Figure 5 reveal that underground structure of the original slope can be divided into four layers from the top to bottom, i.e. (i) the top soft soil layer with a depth of 5~10 m, V_S≈160 m/s~200 m/s, Q_4 and Q_3 loess; (ii) the second layer with a depth of 7~14 m, V_S≈200 m/s~300 m/s, Q_3 loess; (iii) the third layer with a depth of 17 m~25 m, V_S≈300 m/s~400 m/s, Q_3 loess; (vi) the fourth harder layer below, $V_{S\geq}$400 m/s, Tertiary red mudstone. The sliding surface is located in the second loess layer of Q_3. The underground water table level is at 2~3 m above Tertiary red mudstone.

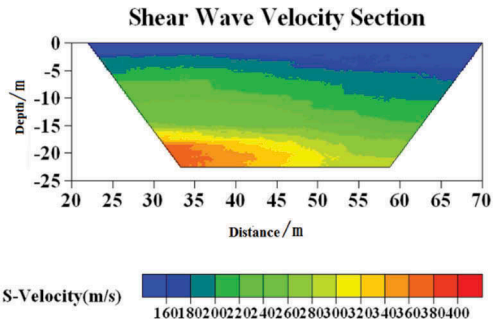

Figure 4. Inversion results of underground Vs structure at the top of slope.

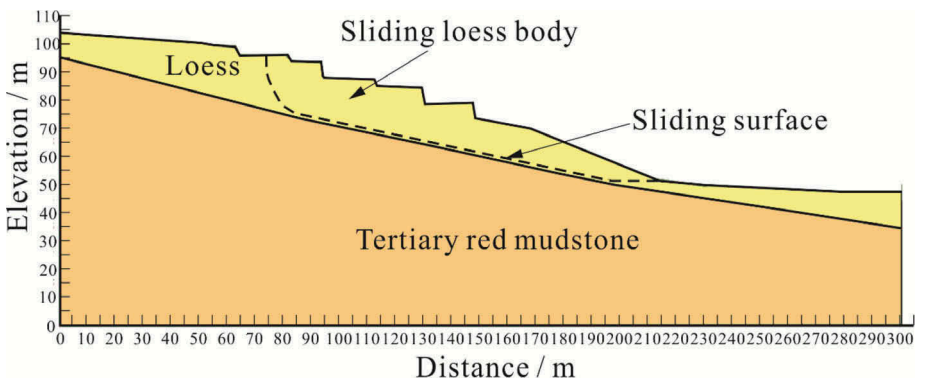

Figure 5. The profile of the western Yongguang landslide.

4 ANALYSIS ON THE MECHANISM OF THE LOESS LANDSLIDE IN YONGGUANG

Particle analysis shown that loess in depth of 8m at the landslide site composes of 20.5% clay, 67.2% silt and 12.3% sand, which is defined as clayey silt or sandy silt. The scanning electron microscopic photographs (SEM) of the same samples revealed that the loess has porous microstructure with weak cohesion shown in Figure 6. This kind of soil has high potential of liquefaction and vulnerability when it is saturated (Wang 2003).

4.1 *The conditions of rainfall, infiltration and soil properties before earthquake*

In order to investigate the influence of rainfall on water content of the slope soil, the daily and accumulative precipitations in the earthquake affected area in the July are presented in Figure 7. As can be seen from Figure 7(a), the number of rainy days in July was 19 days, accounting for 63% of the entire month. Among them, before the earthquake (before July 22), the number of rain days was 15 days, and the rainfall reached 279.6mm, accounting for 84% of the total rainfall in July. It also can be seen from Figure 7 that during the 20 days before the earthquake, two periods of light rain, moderate rain and heavy rain occurred in the earthquake affected area. One rainstorm occurred on July 8, and another heavy rain occurred on the day just before the earthquake. It can be seen from Figure 7(b) that the rainfall intensity in the second stage is greater than that in the first stage. In the first stage, the intensive rainfall is dominated by light rain, while in the second stage, the intensive rainfall is dominated by moderate rainfall. It can be found that the pre-earthquake rainfall process recurs in the pattern of dense multi-day light rain, moderate rain and independent single-day heavy rainfall. Intensive light rain and moderate rain are favorable for rainfall infiltration, and heavy rain has a strong erosion effect on the surface. Therefore, the rainfall process before the

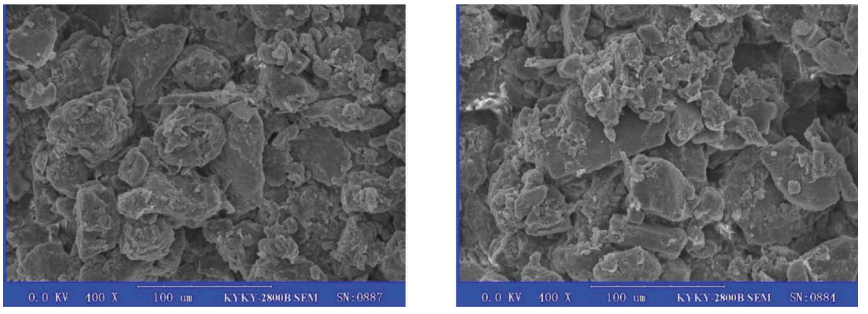

Figure 6. The SEM of loess microstructure in the western Yongguang landslide site.

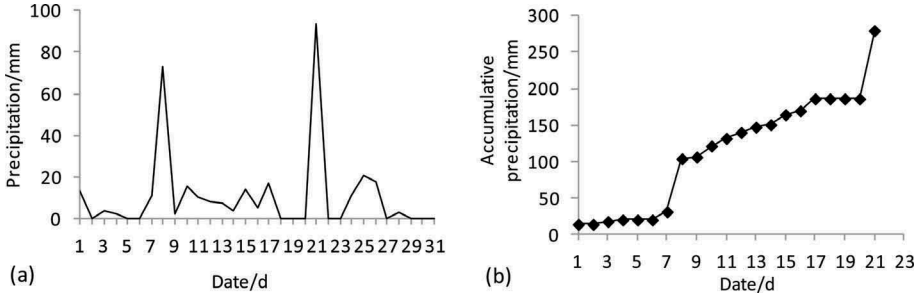

Figure 7. Daily and accumulative precipitations in the earthquake affected area in the July.

earthquake not only increased water content of loess deposit but also supplied underground water through the vertical fissures in loess deposit.

According to the in-situ rainfall infiltration test conducted on a loess slope (Pan, J.Y. et al. 2018), the top layer loess may nearly saturated even if the depth of infiltration is usually less than 2m after a heavy rain or continuous rain for several days. However, raining water infiltration could go down even deeper to the end of fissures once there are vertical fissures in slope soil deposit. Therefore, the continuous rainfall combined with two high-intensity torrential rains before the Minxain-Zhangxian 6.6 earthquake might be sufficient to provide saturation condition for liquefaction of the top loess layer of the slope within 2m or deeper. The site survey shown that the sliding surface developed in the saturated Q_3 loess layer within 2~3m above the red mudstone and the top soil layer was nearly saturated when the earthquake occurred.

4.2 *Strength weakening behavior of loess under infiltration*

In order to investigate the influence of water on shear strength of loess, CU traxial tests and dynamic triaxial tests were performed on undisturbed loess specimens secured from the same depth of 2m in in-situ rainfall infiltration test site. The physical parameters of loess specimen displayed in Table 1.

The influence of water on strength parameters of the loess specimens are illustrated in Figure 8. It can be seen that both the cohesion C and the internal friction angle φ decrease dramatically with the increase of water content. The relationship between strength parameters and water content can be fitted by the following negative exponential attenuation formula (1) and linear attenuation formula (2).

$$C = 69.16 \exp(-0.081\,\omega) \tag{1}$$

$$\varphi = -0.6444\omega + 40.01 \tag{2}$$

Where C is the cohesion of loess, φ is the internal friction angle of loess, and ω is water content. Based on formula (2), the profile of landslide and Vs data, the numerical simulations was carried out on a simplified two-dimensional finite element slope model. The results shown that under the effect of earthquake with an intensity of VIII degree, the displacement of the whole sliding body shows a shear response with a maximum relative displacement of 80cm. The equivalent plastic strain characteristics of the top soil are consistent with the dynamic response characteristics.

Table 1. Physical properties of loess specimen

Pore ratio	Water content %	Dry density g/cm^3	Permeability coefficient cm/s	Grain composition/%		
				Clay	Silt	Sand
1.1	5	1.33	0.0005	11.9	80.1	7.9

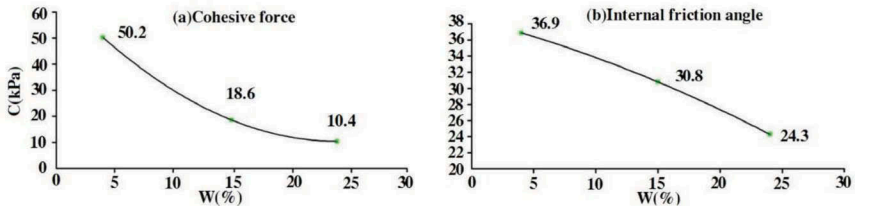

Figure 8. Relationship between strength parameters and water content

4.3 *Dynamic triaxial liquefaction test of landslide soil*

Loess liquefaction can cause land subsidence under flat terrain conditions, and form a mudflow landslide in a slope, even a gentle slope. And it occurs under the action of earthquakes with lower-intensity, resulting in soil slip, mudflow and landslides with highly damaging (Ishihara et al. 1990; Wang et al. 2011; Xu et al. 2016).

In order to investigate if the landslide body liquefied during the earthquake, the two groups of soil samples respectively secured from the depth of 5m at the back wall and the depth of 15m at the bottom of the landslide body in were performed liquefaction tests on the WF-12440 dynamic triaxial torsional shear test system in the Key Laboratory of Loess Earthquake Engineering, Earthquake Administration of China.

4.3.1 *Experimental equipment and methods*

WF-12440 dynamic triaxial torsional shearing instrument is a full-programmed control dynamic and static triaxial torsional shearing instrument produced by British WF Company, which can realize dynamic and static testing on soil specimens under normal and complex stress conditions. The main technical parameters of the instrument are presented in Table 2.

The tests strictly followed the SL237-1999 «Geotechnical Test Code». The preparation specifications of the samples are as follows: solid cylindrical soil samples with a size of Φ50 mm×100 mm, and tests with three steps: saturation, consolidation and cyclic shearing. The low back pressure saturation method was adopted and the pressure was controlled within 100Kpa. Considering the metastable structure and strength characteristics of loess, the self-weight collapsing could occur when the loess meets water. In order to minimize the axial deformation of the specimen, the saturation time was controlled within 90 minutes. The isostatic consolidation was used for consolidation, and the axial consolidation pressure σ_1 was applied according to the formation pressure calculated from the thickness of the landslide body. The dynamic stress applied during cyclic shearing was a sine wave with a frequency of 1 Hz, and its amplitude was set according to the peak ground acceleration. The consolidation and liquefaction tests of the samples were carried out under undrained conditions. The curves of dynamic stress, dynamic strain and dynamic pore water pressure were recorded during cyclic loading. The strain criterion is adopted as the failure criterion for liquefaction of saturated loess (Wang et al. 2003), i.e. pore pressure ratio $U_d/\sigma_0 > 0.2$, and axial strain ε_d reaches 3%.

Table 2. Main technical parameters of WF-12440 test system

Loading mode	Pneumatic actuator
Pressure chamber and manner of applying back Solid cylindrical soil	Pneumatic water system
sample size	Φ50×100mm
Maximum vertical load	±10
Minimum measurable load	1N
Strain measurement accuracy	10^{-5}(0.001%)
Maximum and accuracy of pore water pressure	1MPa, 0.1kPa
Maximum and precision of backpressure	1MPa, 0.1kPa
Maximum value and accuracy of sample volume variation	100cc, 0.1cc

Table 3. Physical index of soil sample

Soil sample Number	Density ρ g/cm^3	Dry density ρ_d g/cm^3	Water content ω %	Initial void ratio e
YG-2*	2.01	1.61	24.53	0.686
YG-3*	1.4	1.35	4.04	1.007

* YG-2: 15m deep at the bottom of the landslides; YG-3: 5m deep at the back wall of the landslide.

4.3.2 *Testing result*

The physical properties of the soil samples, and conditions and results of dynamic triaxial tests on liquefaction are respectively shown in Tables 3 and 4.

The time histories of dynamic stress, dynamic strain and dynamic pore water pressure recorded in dynamic triaxial liquefaction tests are shown in Figure 9.

The test results show that the long-term rainfall before the earthquake made the water content of the slope up to 24.53% and supplied underground water. The sliding surface of the loess slope at 2~3 m above the red mudstone was saturated with underground water and top layer of the slope was nearly saturated, which provided the condition of loess liquefaction in water content. The test result of YG-2 specimen shown that the loess layer around the sliding surface might liquefied under dynamic loading of 25 kPa with cyclic times of 25, where the ratio of pore water pressure increases above 0.2, the amplitude of dynamic strain goes up to 3% dramatically, and liquefied loess layer became a sliding surface. Then the overburden loess deposit slid down along the surface. The test result of YG-3 specimen shown that the top loess layer of the slope might also liquefied under dynamic loading of 30 kPa, which is slightly larger than YG-3 due to a dynamic stress attenuation with a depth of loess layer. But its cyclic times of liquefaction is only 3, which means liquefaction of the top loess layer might come earlier than the sliding surface. Anyway, the liquefied loess mass on the top layer of the slope easily changed into mudflow during sliding down along the slope and the gully and ran faster at the front edge of landslide, which may be verified with the larger residual strain of nearly 15% corresponding to the pore

Table 4. The conditions and results of liquefaction tests

Soil sample Number	Confining pressure σ_3 kPa	Dynamic stress σ_d kPa	Saturation *Sr* %	Water content ω %	Cyclic times of failure N_f
YG-2	138	28	98.60	25.01	25
YG-3	138	32	92.39	34.34	3

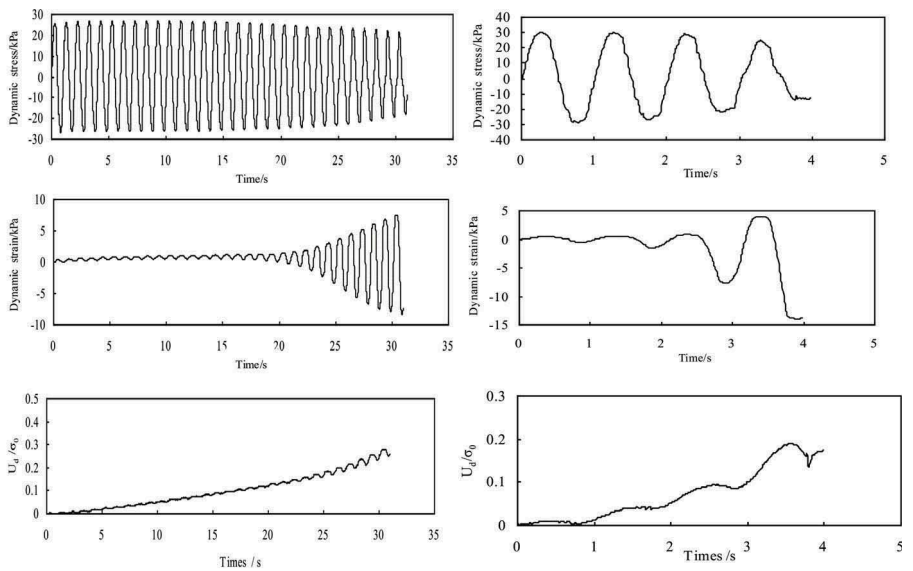

Figure 9. The time histories of dynamic stress, dynamic strain and dynamic pore water pressure.

water pressure ratio of 0.2. Furthermore, the sliding soil mass may run more far due to its attenuated shear strength with water content. Therefore, the western Yongguang loess landslide is a typical liquefaction-triggered mudflow with the characteristics of fast sliding speed, long slip distance and mud-like fluidity under the coupling effect of earthquake and rainfall.

5 CONCLUSION

1. The continuous moderately strong rainfall before the earthquake made the top layer of the slope nearly saturated with water content of 24.53% and the shear strength of the slope soil decrease predominantly. The exposed original site of the back wall of the landslide revealed that the development of the mountainous spring also supplied underground water that cannot be ignored in inducing the slope instability.
2. Under the effect of dynamic loading simulating earthquake intensity of VIII degree, liquefaction might develop in both the sliding surface and top layer of the western Yongguang landslide with the obvious failure phenomenon of dynamic stress attenuation, increasing of both dynamic residual strain and pore water pressure significantly, which triggered the mudflow.
3. Numerical simulations based on the law of dynamic strength parameters attenuating with water content show that under the effect of earthquake, the displacement of the whole sliding body shows a shear response with a maximum relative displacement of 80cm. The equivalent plastic strain characteristics of the soil are consistent with the dynamic response characteristics. The calculated sliding surface is consistent with the field investigation after the earthquake.
4. The landslide in the loess slope caused by the coupling effect of rainfall and earthquake may generate a mudflow which can run much more far distance than common seismic landslides, usually 1km or more, which is more destructive.

ACKNOWLEDGEMENTS

This paper is financially supported by National Natural Science Foundation of China (No.51478444, No.41472297), and the Scientific Research Foundation for the Introducing Talent of Nanjing Tech University.

REFERENCES

Bromhead, E.N. 1994. The stability of slopes [M]. USA: Surrey University Press.

Che, A.L. Wu, Z.J. Peng, D. et al. 2013. Surface wave investigation and dynamic stability analysis for earthquake-induced loess landslides [J]. China Earthquake Engineering Journal, 35(4): 724–729.

Ishihara. Okusa, S. Oyagi, N. et al. 1990. Liquefaction induced flow slide in the collapsible loess deposit in soviet Tajik[J]. Soils and Foundations, 30(4): 73–89.

Li, R.J. Zheng, W. Wang, L.P. Shao S.J. 2011. Progress and Developing Trend on Stability Analyses of Unsaturated Soil Slope [J]. NORTHWESTERN SRTSMOLOCTTAL JOURNAL, 33(S1), 2–9.

Lin, H. Xiong, W. Li, Z.M. 2013. Embedded program for slip surface by shear strain of slopes and parametric analysis [J]. Chinese Journal of Geotechnical Engineering, 35(S1): 52–56.

Pan, J.Y. Hou, D.Y. Li, R.J. et al. 2018. Rainfall infiltration test and analysis of loess slope under different rainfall intensities [J]. Journal of Engineering Geology, 26(5): 1170–1177.

Wang, J.D. Bai, M.X. Xiao, S.F. 2001. A study on compound mechanism of earthquake-related sliding displacements on gently inclined loess slope [J]. Chinese Journal of Geotechnical Engineering, 23(4): 445–449.

Wang, L.M. Wu, Z.J. 2013. Earthuake damage characteristics of the Minxian-Zhangxian Ms6.6 Earthquake and Its lessons [J]. China Earthquake Engineering Journal, 35(3): 401–412.

Wang, L.M. 2003. Loess dynamics, [M]. China: Seismological Press.

Wang, Q. Wang, L.M. Wang, J. et al. 2017. Prediction of loess earthquake disasters in the reconstruction sites after the Minxian-Zhangxian M.6.6 earthquake [J]. HYDROGEOLOGY & ENGINEERING GEOLOGY, 44(5):137–142.

Wu, Z.J. Che, A.L. Chen, T. et al. 2010. Test Study and numerical analysis of seismic response of pile foundation of bridge at permafrost regions along Qinghai-Tibet railroad[J]. Rock and Soil Mechanics, 31(11): 3516–3524.

Xi, C. Q. Hu, Z.A. Zhang, P.S. 2018. Analysis of spectral characteristics and exploration depth of vibro-seis-random source [J]. Progress in Geophysics, 33(4):1734–1739.

Xu, Q. Peng, D.L. et al. 2016. DangChuan 2~# Landslide of april 29, 2015 in Heifangtai area of Gansu province: failure characteristics and mechanism [J]. Journal of Engineering Geology, 24(2): 167–180.

Yuan, Z.X. Wang, L.M. Wang, P. 2004. Further Study on Mechanism and Discrimination Criterion of Loess Liquefaction [J]. Earthquake Engineering and Engineering Vibration, 24(4): 164–168.

Yamanaka, H. Ishida, H. 1996. Application of genetic algorithms to an inversion of surface wave dispersion data[J]. Bulletin of the Seismological Society of America, 86(2): 436–444.

Zhang, Y.C. Yang, G.H. 2013. Searching for critical slip surface in soil slopes based on calculated results by variable modulus elastoplastic strength reduction method[J]. Chinese Journal of Geotechnical Engineering, 35(S1): 14–22.